

Assessment of the High-frequency Response in Railway Pantograph-Catenary Interaction Based on Numerical Simulation

Yang Song, *Member, IEEE*, Anders Rønquist, Petter Nāvik

Abstract—The numerical model is a well-acknowledged tool to evaluate railway pantograph-catenary interaction performance. The current standard restricts most current simulation tools by a cut-off frequency of 20 Hz. This low-frequency range of interest cannot fully describe the current collection quality of pantograph-catenary. This paper includes simulation with cut-off frequencies up to 200 Hz to investigate the high-frequency behaviour of pantograph-catenary interaction. The reference model of pantograph-catenary in the benchmark is taken as the analysis object. Firstly, the effect of key simulation parameters of the resulting contact force is investigated. A small element length in the finite element model is proposed to prevent the frequency range of interest being contaminated by the numerical error. The contact stiffness has an opposite effect on the contact force in low and high-frequency ranges. Then the source and the amplification factor of high-frequency components of contact force are investigated. The results show that the half and quarter of the dropper/steady arm interval length presents the primary source of high-frequency components of the contact force. The corresponding wavelength can also be found in the high-order modes of the catenary. Finally, a variable time step procedure is also proposed to capture the contact loss occurring at high frequencies accurately. The comparison of the results between the variable and constant time steps indicates that the traditional constant time step may result in errors when calculating the contact loss duration.

Index Terms—Electrified railway, Current collection quality, High-frequency, Pantograph-catenary interaction, Variable time step

I. INTRODUCTION

In electrified rail operations the electric power is transmitted from the catenary to the locomotive via the sliding contact with a pantograph installed on the train roof, as shown in Fig. 1. The pantograph is often the only source of power transmission for electric trains. The interaction performance of pantograph-catenary is thus of critical importance, as it directly determines the current collection quality and restricts the maximum operating speed. As the rapid expansion of high-speed network all over the world in the last several decades, the revelation, evaluation and optimisation of pantograph-catenary interaction performance have attracted ever-increasing attention from both academy and industry.

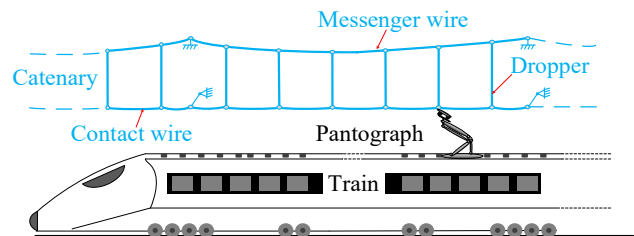


Fig. 1. Schematic of a pantograph-catenary system

A. Problem description

In order to ensure an excellent current collection quality, a stable contact force is desired between the pan head and the contact wire. An excessive contact force worsens the wear and fatigue of the contact surface, and even damage the contact wire. In contrast, an inadequate contact force increases the possibility of occurrence of contact loss, which results in frequent arcing [1] and even the interruption of electrical supply. Therefore, the contact force is the most important indicator to assess the interaction performance of pantograph-catenary. According to EN 50367 [2], the current collection quality is mainly evaluated by some time-domain statistics of contact force, which are low-pass filtered at 20 Hz due to the limitation of detection and simulation techniques. The traditional view is that this low-frequency range is enough to describe the critical implication of the catenary geometry on the contact force. Usually, the span length of a catenary is around 40-65 m, and the dropper spacing is around 5-6 m. The current top operating speed is 350 km/h across the world, and the corresponding span-length and dropper-spacing frequencies are around 1.50-1.62 Hz and 16.20-19.44 Hz, respectively, which are covered by the current low-pass frequency 20 Hz [3]. This frequency range of interest is also enough to adequately describe the rigid body motions used to compensate for between measuring the force under the pan head and calculating the contact force. Thus, this frequency of interest is widely adopted in most numerical models [4]. With the recent improvement of the understanding of the pantograph-catenary dynamics, the high-frequency behaviours are also of great importance for the assessment of current collection quality. Some realistic short-wavelength disturbances (such as the wear and cant in the contact wire) have a direct impact on the contact force at up to

100 Hz [5]. The high-order deformation modes of the contact wire are also contributing factors affecting the high-frequency performance. Some phenomena happening at high frequencies are critical for evaluating the current collection quality. For instance, EN 50367 [2] specifies that the minimal contact loss duration is 0.005 s. Thus, to fully describe the contact loss phenomenon, the numerical models should be validated up to 200 Hz.

B. Literature review

As is well known, numerical models are efficient tools to evaluate the pantograph-catenary interaction performance, compared with the tremendous cost of laboratory and field tests. Especially in the design phase, the numerical simulation is helpful to validate the design strategy and optimise the structural parameters. Therefore, the accuracy of the numerical model to reproduce the realistic phenomenon is of great interest to the scientific and industrial communities. The catenary is customarily comprised of many tensioned cables exhibiting significant pre-stress and nonlinearity. The finite element method is the most preferred approach to model the catenary. Lopez-Garcia et al. [6] utilise an analytical cable equation to calculate the initial configuration of catenary based on Newton-Raphson method. Tur et al. [7] propose a shape-finding method for computing the equilibrium state based on the absolute nodal coordinate formulation (ANCF). Song et al. [8] present a nonlinear modelling method for catenary based on the explicit formula of cable and truss elements. Considering realistic disturbances to the catenary, the wind load [9], aerodynamic instability [10] and vehicle-track perturbation [11] are included in the numerical models to evaluate their effects on the pantograph-catenary interaction. To reproduce the realistic defects of catenary, the contact wire irregularities [12], [13], dropper defect [14] and wear [15] are included in the assessment of current collection quality. To ensure the accuracy of simulation results, the measurement data from field tests are utilised to modify [16] and validate [17], [18] the numerical models. The hardware-in-the-loop technique has been widely developed to couple a mimic catenary and realistic pantograph [19], which provide more convincing measured results to analyse the pantograph behaviour. To improve the simulation efficiency, some simplifications are made based on the idea of moving mesh [20], [21] and linearisation [22] without affecting the simulation accuracy. Base on numerical models, the influence of some critical parameters, such as the tension [23], pantograph interval [24], and catenary geometry [25] on the interaction performance are analysed.

The frequency of interest for the evaluated contact forces obtained by numerical simulations is normally limited to 0-20 Hz. This is manifested in the latest benchmark [26], in which ten mainstream simulation tools of pantograph-catenary interaction are compared to establish a validation benchmark for up to 20 Hz. Recently, this low-frequency range of interest has been challenged by several scholars [27], [28], as it is not enough to fully describe the current collection quality. The effect of short-wavelength disturbances, the high-order deformation mode of contact wire and some critical high-frequency phenomena (such as the contact loss and arcing) have

important implications on the current collection quality. Therefore, the cut-off frequency is necessary to move up for both online detection and numerical simulations. When the frequency of interest moves up, the numerical algorithm validated for low-frequency may not be still valid for simulating high-frequency response. It has been indicated in [29] that the catenary modelled by cable element cannot describe the wave dispersion happening at over 50 Hz. Therefore, the beam element is widely adopted to include the effect of bending stiffness. Some simulation parameters, such as the time step, element length and contact stiffness in the previous numerical models, should be updated for higher frequencies. In order to accurately capture the contact loss occurring at high frequencies, a very tiny time step should be adopted to improve the sampling frequency, which may bring tremendous computational cost. In order to improve efficiency, most current simulation models adopt low sampling frequencies (normally no more than 1000 Hz [26]) in their simulations. In this way, the traditional constant time step integration scheme is not able to accurately capture the time instance of the separation and the reattachment between the pan head and the contact wire, which renders some errors when calculating the contact loss duration. Therefore, a variable time step is desired to properly describe the contact loss occurring at up to 200 Hz with a relatively low sampling frequency. Furthermore, the physical meanings of high-frequency components of the contact force are still not clear. Fundamental research on the high-frequency response of contact force is thus justified to be conducted.

C. Contribution and scope

Addressing the shortcomings in previous researches, this paper focuses on the analysis of the high-frequency behaviour of pantograph-catenary interaction via numerical simulations. The ANCF beam element is utilised to model the catenary. In order to fully describe the contact loss occurring at high frequencies, the frequency range of interest in the simulation is set up to 0-200 Hz. Without loss of generality, the reference model in the benchmark [26], which has been validated for 0-20 Hz is adopted to conduct the analysis. Firstly, the key simulation parameters such as the mesh size and contact stiffness are discussed for the high-frequency stimulation. Then the high-frequency components of contact force are analysed to make sense of their physical meanings. Finally, a variable time step integration scheme is proposed to accurately capture the contact loss duration occurring at high frequencies without having to use an extremely high sampling frequency, which is shown necessary when using only constant time step. The resulting contact forces obtained by the variable and constant time steps are compared to indicate the necessity of using a variable time step.

II. MODEL OF PANTOGRAPH-CATENARY SYSTEM

In this work, a reference model of the pantograph-catenary system in the benchmark [26] is utilised to investigate its high-frequency behaviour. The catenary is modelled by ANCF, and the pantograph is considered as a lumped mass model. The details of the modelling approach are described in this section.

Table 1. Static validation of present model against benchmark

Dropper No.	Pre-sag			Elasticity		
	Benchmark (mm)	Present (mm)	Error (%)	Benchmark (mm/N)	Present (mm/N)	Error (%)
Sup	0	0	0	0.206	0.19257	6.52
1	0	0	0	0.165	0.15647	5.17
2	24	24.00	0	0.273	0.26774	1.93
3	41	41.00	0	0.345	0.3268	5.28
4	52	52.00	0	0.388	0.36832	5.07
5	55	55.00	0	0.4	0.37509	6.23
6	52	52.00	0	0.388	0.36832	5.07
7	41	41.00	0	0.345	0.3268	5.28
8	24	24.00	0	0.273	0.26774	1.93
9	0	0	0	0.165	0.15647	5.17
Sup	0	0	0	0.206	0.19257	6.52

Table 2. Dynamic validation of present model against benchmark

	Benchmark	Present model	Error
F_m [N]	169	169.15	0.09%
σ (0-20 Hz) [N]	53.91	52.59	2.45%
σ (0-2 Hz) [N]	38.27	38.25	0.05%
σ (0-5 Hz) [N] ^b	41.04	41.00	0.10%
σ (5-20 Hz) [N] ^b	34.80	32.99	5.20%
F_{max} [N]	313.22	305.85	2.35%
F_{min} [N]	60.40	56.22	6.9%

in which, \mathbf{M}_C^G , \mathbf{C}_C^G and $\mathbf{K}_C^G(t)$ are the mass, damping and stiffness matrices, respectively. $\mathbf{F}_C^G(t)$ is the external force vector which contains the contact force and gravity.

B. Modelling of pantograph and contact

The pantograph is represented by a three-stage lumped mass model as depicted in the benchmark [26]. The interaction between the pan head and the contact wire is modelled by a penalty function method based on the assumption of the relative penetration δ on the contact surface. The contact force f_c is calculated by the product of the contact stiffness k_s and the penetration δ as follows:

$$f_c = \begin{cases} k_s \delta & \text{if } \delta > 0 \\ 0 & \text{if } \delta \leq 0 \end{cases} \quad (9)$$

With the help of Eq. (9), the equation of motion for the coupling pantograph-catenary system is written by

$$\mathbf{M}^G \ddot{\mathbf{U}}(t) + \mathbf{C}^G \dot{\mathbf{U}}(t) + \mathbf{K}^G(t) \mathbf{U}(t) = \mathbf{F}^G(t) \quad (10)$$

in which, \mathbf{M}^G , \mathbf{C}^G and $\mathbf{K}^G(t)$ are the mass, damping and stiffness matrices for the whole system, respectively. $\mathbf{F}^G(t)$ is the external force vector. A Newmark integration scheme is adopted to solve Eq. (10). The stiffness matrix $\mathbf{K}^G(t)$ is updated in each time step to fully describe the nonlinearity of the system.

C. Validation of model

The mean values of the results obtained by the ten different software in the world are utilised to validate the accuracy of the

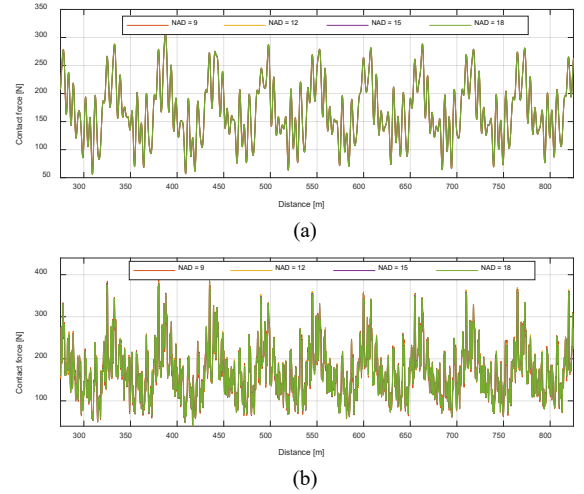


Fig. 4. Contact force with different NADs (a) low-pass filtered by 20 Hz; (b) low-pass filtered by 200 Hz

present model. The world benchmark provides the results for both static and dynamic validations [26]. In the static validation, the pre-sag and elasticity of the contact wire obtained by the present model are compared with the benchmark in Table 1. It shows that pre-sag obtained by the present method is exactly the same as the benchmark. The maximum error of the elasticity is just 6.52%, which is much lower than the threshold 10%. The dynamic validation is implemented by comparing the key contact force statistics with the benchmark. As shown in Table 2, the results of the present model show good consistency with the benchmark. However, it should be noted that this validation is just valid for up to 20 Hz. The high-frequency behaviour is not involved in the benchmark.

III. SIMULATION PARAMETERS FOR HIGH-FREQUENCY

When the frequency of interest increases, the numerical algorithm validated for low-frequency range may not be valid for simulating high-frequency response. In this section, the effect of two key simulation parameters (mesh size and contact stiffness) on the simulation results are investigated. The analysis model of catenary has 17 spans, and the 10 central spans are selected as the analysis object to avoid the boundary effect. The train speed is set to as 320 km/h in the following analysis.

A. Mesh size

Four types of element length are adopted to perform numerical simulations. The element length is defined by the number of nodes between two adjacent droppers (NAD). Using different element lengths, Fig. 4 (a) and (b) present the contact forces with a low-pass filtered frequency of 20 Hz and 200 Hz, respectively. In Fig 4 (a), when the contact force is low-pass filtered at 20 Hz, no significant difference can be found among different element lengths. However, when the frequency increases, the effect of element length on the contact force time-history becomes significant, as shown in Fig. 4 (b). This phenomenon is also observed in Fig. 5, which shows the contact force standard deviations with different NADs and cut-off frequencies. For the cut-off frequencies of 20 Hz and 100

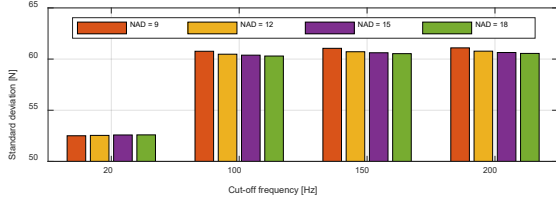


Fig. 5. Contact force standard deviations with different NADs and cut-off frequencies

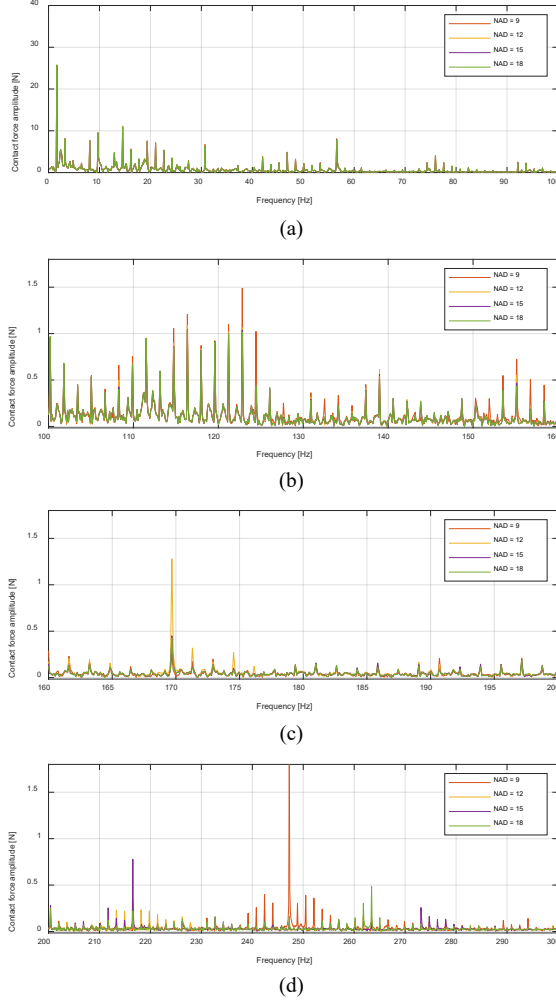


Fig. 6. Contact force spectrums with different NADs at: (a) 0-100 Hz; (b) 100-160 Hz; (c) 160-200 Hz; (d) 200-300 Hz

Hz, the contact force standard deviations do not exhibit big difference with different NADs. However, when the low-pass frequency increases, the contact force standard deviations with longer element length are higher than the results with smaller element length. For all cut-off frequencies, the results with NAD = 15 are similar to NAD = 18. Figs. 6 (a-d) show the frequency spectrums of contact force with the frequency range of 0-100 Hz, 100-160 Hz, 160-200 Hz, and 200-300 Hz respectively. In Fig. 6 (a), it is seen that for 0-100 Hz, the spectrums of contact force with different element lengths are almost the same. The significant difference appears in Fig. 6 (b), in which the spectrum amplitude with NAD = 9 is much higher than others at around 123 Hz and 157 Hz. When a moving load traverses along a finite element beam, the element length is able to introduce a disturbance with the specific

wavelength same to the element length. This periodic disturbance is generated by the interpolation of the displacement between two nodes. The frequency f_c of this type of disturbance can be calculated by

$$f_c = n \frac{v}{L_e} \quad (n = 1, 2 \dots N) \quad (11)$$

in which, L_e is the element length. v is the train speed. With NAD = 9, there are two element lengths of 0.56 m and 0.72 m. By substituting into Eq. (11), it can be shown that the corresponding frequencies are 123.67 Hz and 158.02 Hz, which are consistent with the spectrum peaks observed in Fig. 6 (b). According to this theory, f_c with NAD = 12 can be calculated as 170.05 Hz and 217.28 Hz, which again can be observed in Figs. 6 (c-d). For NAD = 15, f_c is calculated as 216.43 Hz and 276.54 Hz, which can be observed in Fig. 6 (d). For NAD = 18, f_c is calculated as 262.80 Hz and 335.80 Hz. The former can be seen in Fig. 6 (d). It should be noted that there is a significant peak at around 250 Hz with NAD = 9 in Fig. 6 (d). This peak is relevant to the half element length, namely $n = 2$ in Eq. (11). In order to correctly reproduce the physical phenomenon, f_c should be out of the frequency range of interest. Therefore NAD = 15 and NAD = 18 can be selected for simulating up to 200 Hz in this case.

B. Contact stiffness

The contact stiffness in Eq. (9) is a parameter introduced due to the contact formulation used in the numerical simulation to couple the pantograph and catenary. The value of the contact stiffness is normally selected based on experience to keep the frequency response functions between the displacements of the contact point considered as belonging to the pan head and the contact wire as close to unity as possible in the frequency range of interest. Therefore, the contact stiffness should be big enough to make the two contact points as tight as possible. But an overlarge value may cause mathematical problems, and cannot lead to accurate results. Normally the contact stiffness is selected within 50000–200000 N/m, which ensures that appropriate results can be obtained at 0-20 Hz [15]. In this section, a sensitivity analysis is conducted to reveal the effect of contact stiffness on the contact force within different frequency ranges of interest.

The simulation conditions are set as the same as the above analysis. Fig. 7 shows the time histories of the two-span contact force at 0-200 Hz with different contact stiffness. It is seen that the contact stiffness does not change the waveform of contact force, but has a direct effect on the amplitude. Figs. 8 (a) and (b) show the contact force spectrums at 0-50 Hz and 50-200 Hz, respectively. In Fig. 8 (a), it is seen that for most peaks, the contact force amplitude decreases with the increase of contact stiffness. However, in the high-frequency range, as shown in Fig. 8 (b), most peaks decrease with the increase of contact stiffness. Similar results can also be seen in Fig. 9, which presents the contact force standard deviations versus contact stiffness with different cut-off frequencies. In the frequency ranges of 0-20 and 0-50 Hz, the contact force standard deviation undergoes a continuous decrease with the increase of contact stiffness. However, when the frequency of interest moves up to 200 Hz, the contact force standard deviation shows a contrary

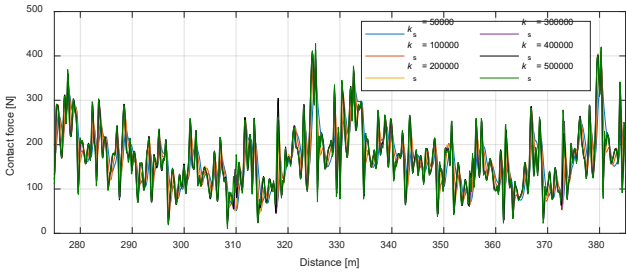


Fig. 7. Two-span contact force at 0-200 Hz with different contact stiffness

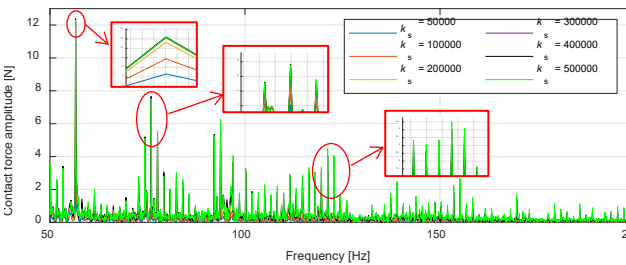
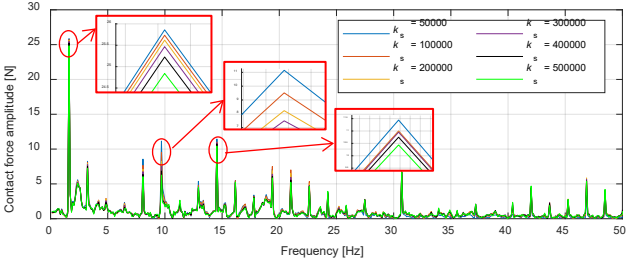


Fig. 8. Contact force spectrum with different contact stiffness with: (a) 0-50 Hz; (b) 50-200 Hz

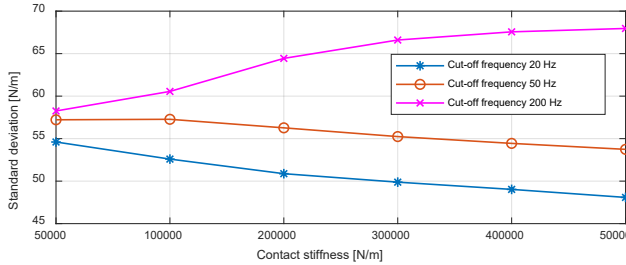


Fig. 9. Contact force standard deviation versus contact stiffness with different cut-off frequency

trend against the low-frequency range. Therefore it is concluded that the contact stiffness has a different effect on the contact force in low and high-frequency ranges. It is also seen that with the increase of the contact stiffness from 50000 N/m to 500000 N/m, the resulting contact force standard deviation shows a difference of 11.94%, 6.08% and 16.67% at 0-20 Hz, 0-50 Hz and 0-200 Hz respectively. The determination of an appropriate contact stiffness requires the high-frequency measurement data as a reference. Therefore, the breakthroughs of the current standard and the current inspection equipment, which limits the measurement frequency within 0-20 Hz are expected to emerge.

IV. HIGH-FREQUENCY COMPONENTS ANALYSIS

From the contact force spectrum given in Fig 8, it is seen that

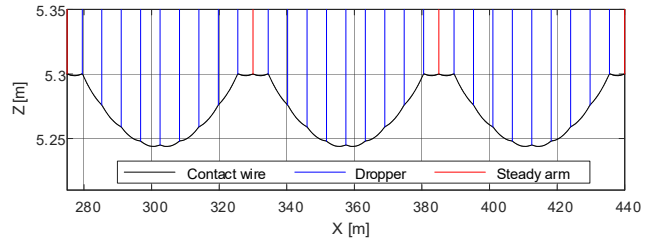


Fig. 10. Contact wire pre-sag

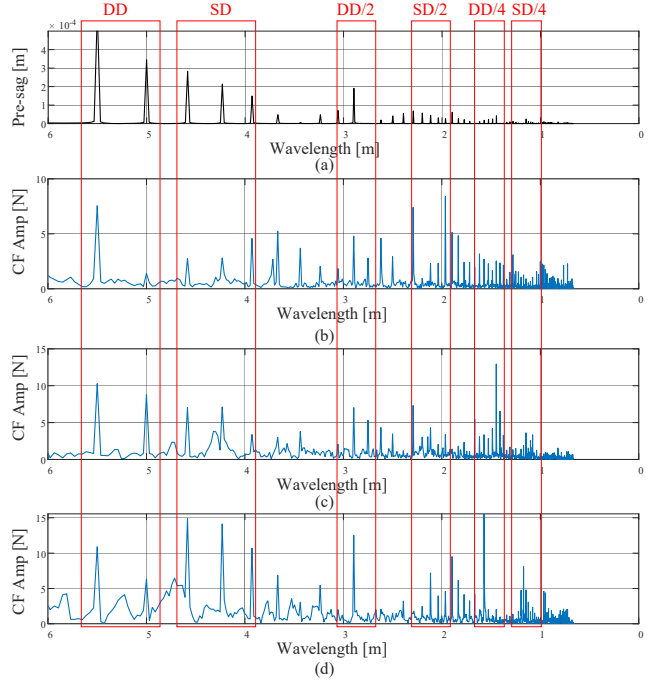


Fig. 11. Spectrums of (a) contact wire pre-sag; (b) contact force at 225 km/h; (c) contact force at 275 km/h; (d) contact force at 320 km/h

there are some components in the high-frequency range. For the traditional low-frequency range, the source of the frequency components is clear. Most of the low-frequency components are directly related to the structural parameters, such as the span length, dropper to dropper interval and steady arm to dropper interval. In this section, the source of the high-frequency components of the contact force is analysed, and the corresponding mode is investigated to determine the amplification factor.

A. Source of the high-frequency component

In the low-frequency range, it has been a common understanding that most frequency components of the contact force are directly determined by the structural parameters. The contact wire configuration is a direct reflection of the structural geometry. As shown in Fig. 10, the contact wire pre-sag exhibits a significant periodicity with respect to the span length, dropper to dropper (DD) interval and the steady arm to dropper (SD) interval. The spectrum of the contact wire pre-sag is shown in Fig. 11 (a). To facilitate a comparison, the contact force spectrums at three different speeds, namely 225 km/h, 275 km/h and 320 km/h are presented in Figs. 11 (b-d). It is seen that the spectrum peaks in the contact force are highly consistent with the peaks in the pre-sag. As the physical

meanings of low-frequency components have been identified by several previous works [30], this work mainly focuses on the identification of the physical meaning in the high-frequency (long-wavelength) range. The spectrum is divided into six regions. The first two regions are at around a wavelength of 5.75 m and 4.25 m, respectively, which are related to the DD and SD interval. The third region is at around the wavelength of 2.88 m, which is related to the half DD interval. The fourth one is at around the wavelength of 2.12 m, which is related to half SD interval. The fifth one is at around the wavelength of 1.44 m, which is related to a quarter of DD interval. The last one is at around the wavelength of 1.13 m, which is related to a quarter of the SD interval. It is also seen that out of the four ranges, the spectrum energy is small and can be neglected. Therefore, it is concluded that the half and quarter of the DD/SD interval present the main source of high-frequency components of the contact force.

B. Amplification factor

This section investigates the catenary mode shapes to determine the sensitive wavelength, which is the amplification factor of the contact force at the specific frequency. The procedure as shown in Fig. 12 is proposed to identify the sensitive wavelength for each mode. Through the Fast Fourier Transformation (FFT) to the vertical mode shape of the contact wire against its longitudinal distance, the spectrum of contact wire mode shape can be obtained. The spectrum peaks represent the sensitive wavelengths of each mode. Among all the modes, it can be found that some of them have the specific sensitive wavelengths equal to DD/2, SD/2, DD/4 and SD/4, which may amplify the excitation from the pre-sag. Figs. 13 (a-b) show the catenary mode shape related to the DD/2 and the corresponding spectrum of contact wire mode shape, respectively. It is seen that a high spectrum peak appears at around the spatial frequency related to DD/2, which may cause the amplification of the contact force amplitude at this frequency. Figs. 14 (a-b) show the catenary mode shape related to the SD/2 and the corresponding spectrum of contact wire mode shape, respectively. This procedure can also establish similar contact wire mode shape spectra associated with the DD/4 and SD/4 by investigating high-order modes of the catenary. These are, due to the similarity, not presented here to save paper space.

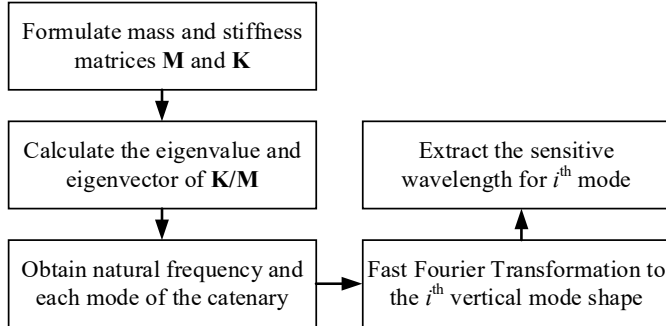


Fig. 12. Extraction of sensitive wavelength for each mode

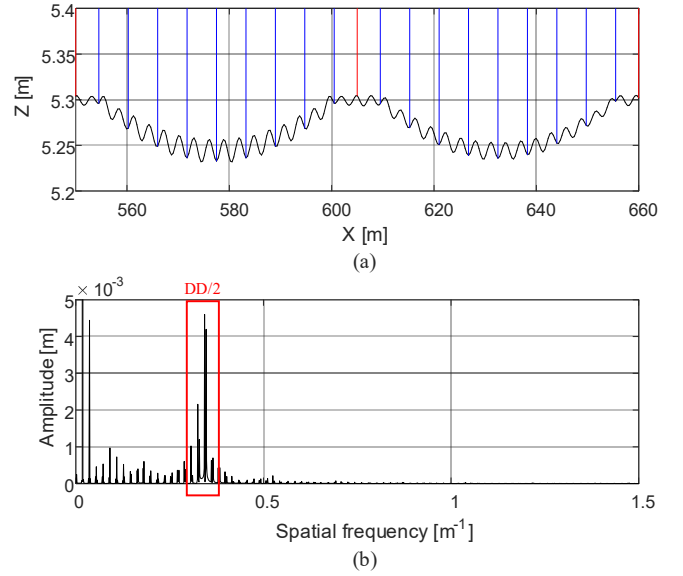


Fig. 13. Catenary mode related to DD/2: (a) model shape; (b) contact wire uplift spectrum

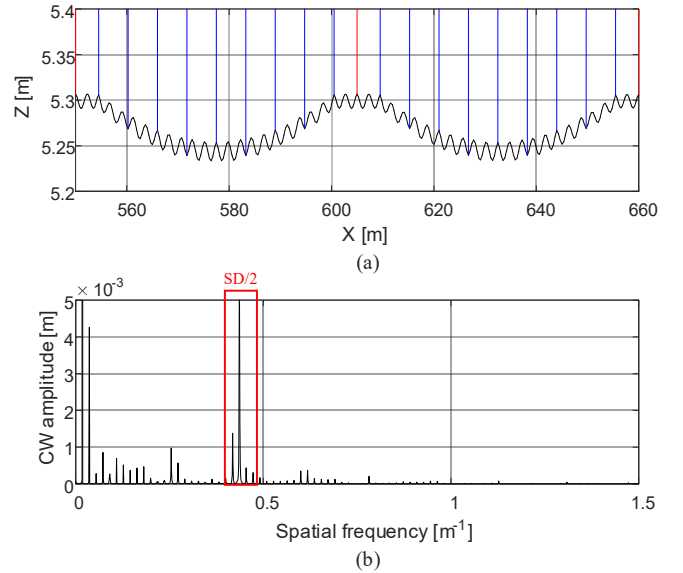


Fig. 14. Catenary mode related to SD/2: (a) model shape; (b) contact wire uplift spectrum

C. Suggesting the frequency range

According to the traditional view, the cut-off frequency of 20 Hz can reflect the effect of structural geometry on the contact force. However, through the analysis in this section, it is seen that the frequency related to a half/quarter of DD/SD have a noticeable effect on the contact force. Thus, in order to fully describe the catenary geometrical effect, the cut-off frequency should move up over than the frequency related to a quarter of DD/SD. For the given case, the contact force standard deviations with different cut-off frequencies are presented in

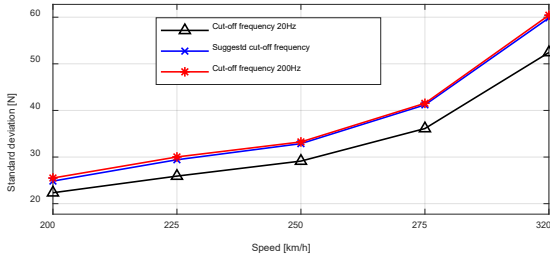


Fig. 15. Contact force standard deviation versus speed with different cut-off frequency

Fig. 15 at different speeds. As the frequency related to $SD/4$ is 0.88 m^{-1} , the suggested cut-off frequency is set to 0.9 m^{-1} . The corresponding temporal frequency is 50 Hz, 56.25 Hz, 62.5 Hz, 68.75 Hz and 80 Hz at 200 km/h, 225km/h, 250km/h, 275 km/h and 320 km/h, respectively. It is seen that the resulting contact force standard deviations filtered at the suggested frequency are very close to the results filtered at 200 Hz. However, the results filtered at 20 Hz are much lower than others, as the low cut-off frequency cannot cover the important implication of the geometrical effect. Therefore, it is concluded that in order to fully describe the geometrical effect, the cut-off frequency should be higher enough to reflect a quarter of DD/SD wavelength.

V. VARIABLE TIME STEP FOR CONTACT LOSS DURATION

The contact loss occurring at high-frequency is an important index to assess the current collection quality. However, the traditional numerical simulation is always implemented with a constant time step (CTS), which may not accurately capture the separation and reattachment time instants. In this section, a variable time step (VTS) is proposed to accurately calculate the contact loss duration.

A. Definition of VTS

As shown in Fig. 16, assume that the contact loss occurs within the time step $t_n \rightarrow t_{n+1}$. If a constant time step Δt is used, the exact separation time instant cannot be captured. To address this shortcoming, a tangent line l is drawn to calculate its intersection point t_{n+1}^b with the time axis. Then the time step is updated to $\Delta t^b = t_{n+1} - t_{n+1}^b$ to calculate the penetration δ at t_{n+1}^b . This procedure can be repeated until a proper penetration $|\delta| < \delta_{\text{critical}}$ is obtained. In this work, the threshold δ_{critical} is defined as 10^{-4} m . A similar procedure is also used to capture the reattachment time instant.

B. Numerical simulation

In this section, the numerical simulations are performed to compare the results of VTS with the traditional constant time step. It should be noted that the simulations in the above sections are conducted in ideal conditions, which cannot reproduce the contact loss in reality. In order to simulate the contact loss, some realistic disturbances should be included in the model. Here, the contact wire irregularity, which is the most common disturbance to the pantograph-catenary interaction, is included in the catenary model. Due to the lack of measurement

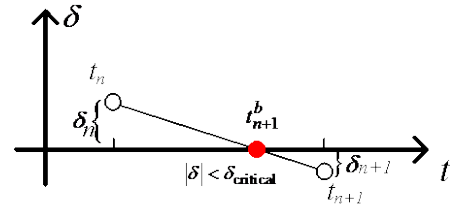


Fig. 16. Description of variable time step scheme

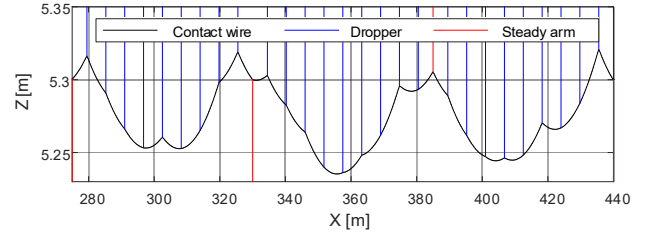


Fig. 17. Contact wire pre-sag with irregularities

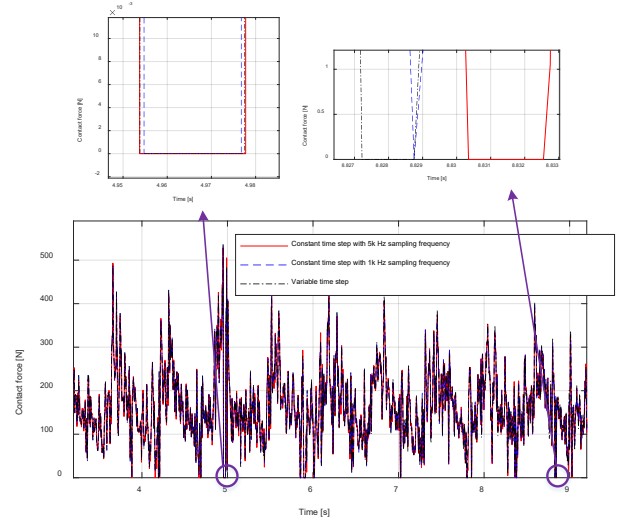


Fig. 18. Comparison of contact force between variable time step and constant time step

data, the contact wire irregularity for this type of catenary is assumed as a set of random uniform number. The initial configuration of the contact wire with irregularities is shown in Fig. 17. Compared with Fig. 10, it is seen that the distortion of the geometry causes significant contact wire irregularities. The other simulation conditions are set as the same as the above sections. The train speed is 320 km/h, and a high sampling frequency of 1000 Hz is adopted in the analysis. In order to show the advantage of the present variable time step, a very high sampling frequency of 5000 Hz is also adopted for the comparison. Fig. 18 presents the evaluated contact forces obtained by the VTS and the CTS with both of 1000 Hz and 5000 Hz sampling frequencies. It is seen that the waveforms of resulting contact forces are generally similar. Only the duration of the contact loss obtained by the three methods is different, as depicted in the locally enlarged views. For the contact loss occurring at around 4.954 s, the contact loss duration of VTS is similar to the result of CTS with 5000 Hz sampling frequency. Whereas, the contact loss duration of CTS with 1000 Hz is much different from others. From the other enlarged view, it is seen that the CTS with 1000 Hz sampling frequency cannot

Table 3. Contact loss duration with variable and constant time step

Contact loss time	1 st	2 nd	3 rd	4 th	5 th	6 th	7 th	8 th	9 th	10 th	11 th	12 th	13 th	14 th	15 th	16 th
CTS 1k [ms]	Not count	Not count	3.00	2.00	22.00	5.99	18.00	7.99	4.00	6.99	2.00	6.99	1.00	2.00	Not count	Not count
CTS 5k [ms]	2.25	1.25	4.10	3.35	23.71	7.39	19.54	7.10	5.06	6.08	1.44	4.03	1.59	3.53	1.67	2.36
VTS [ms]	Not count	Not count	4.14	3.32	23.68	7.33	19.37	6.99	5.19	6.10	1.42	3.98	1.53	3.58	1.41	2.00
Error to 1k [%]			27.54	39.76	7.09	18.28	7.07	14.31	22.93	12.73	40.85	75.63	34.64	44.13		
Error to 5k [%]			0.97	0.90	0.13	0.82	0.88	2.86	2.50	3.28	1.41	1.26	3.92	1.68	18.44	18.00

capture the contact loss occurring at 8.828 s. The position of the evaluated contact loss duration by VTS is a bit different from the result of CTS with 5000 Hz sampling frequency, which is caused by the limitation of low sampling frequency. The VTS is able to improve the accuracy to evaluate the contact loss duration, but cannot reflect behaviours that need higher sampling frequencies to be described. This conclusion is also demonstrated in Table. 3, where each contact loss duration obtained by the three methods are presented. It is seen that two contact losses evaluated by CTS with 5000 Hz are not captured by the VTS due to the limitation of sampling frequency. When the CTS with 1000 Hz sampling frequency is adopted to calculate the contact loss duration, the maximum error with respect to the VTS can reach 75.63%. Even two times the contact loss, which is described by the VTS and CTS with 5000 Hz sampling frequency is not captured by CTS with 1000 Hz sampling frequency. In contrast, the error of CTS with 5000 Hz sampling frequency with respect to VTS is no more than 20%. According to EN 50367 [2], the simulation tool can be used to evaluate the contact loss rate. However, a very high sampling frequency should be used to accurately capture the contact loss duration, which causes tremendous computational cost. Using the variable time step is an efficient and economical way to accurately reproduce this physical phenomenon occurring at high-frequencies. From the numerical results in Table. 3, it is seen that even though a high sampling frequency up to 1000 Hz is used, some significant differences of evaluated contact loss duration can be seen between the constant and variable time steps.

VI. CONCLUSIONS

The simulation of high-frequency behaviours of pantograph-catenary interaction is of great importance to improve the understanding of pantograph-catenary dynamics and accurately evaluate the quality of the current collection. The previous numerical algorithms validated at up to 20 Hz may not be directly used for simulating high-frequency behaviours. In this paper, the effect of some key simulation parameters (including mesh size and contact stiffness) on the resulting contact force at high frequencies is analysed. The source and amplification factor of high-frequency components of the contact force are investigated. Finally, a variable time step procedure is proposed to properly capture the contact loss occurring at high frequencies. The main conclusions are drawn as follows:

1) The element length related frequency v/L_e should be out of the frequency range of interest to avoid the contamination of the results.

2) The contact stiffness has an opposite effect on the contact

force in low and high-frequency ranges. The increase of contact stiffness causes the decrease of contact force fluctuation in low-frequency range but the increase of contact force fluctuation in high-frequency range.

3) The half and quarter of the DD/ SD interval present the main source of high-frequency components of the contact force. The corresponding structural wavelength can also be found in high-order catenary modes.

4) In order to fully describe the geometrical effect, the cut-off frequency should be higher enough to reflect a quarter of DD/SD wavelength.

5) A variable time step is an efficient approach to accurately capture the contact loss duration occurring at high-frequencies without a very high sampling frequency, which definitely leads to considerable computational cost.

Apart from the factors affecting high-frequency response included in this paper, other factors such as the vehicle vibrations, anomalies of pantograph-catenary and wind loads disturbances also contribute to the high-frequency response. The non-stationary response caused by the stochastic disturbance at high-frequency deserves more attention in the authors' future works

REFERENCES

- [1] S. Midya, D. Bormann, Z. Mazloom, T. Schütte, and R. Thottappillil, "Conducted and radiated emission from pantograph arcing in AC traction system," *2009 IEEE Power Energy Soc. Gen. Meet. PES '09*, pp. 1–8, 2009.
- [2] EN 50367, *Railway applications - Current collection systems - Technical criteria for the interaction between pantograph and overhead line*, no. August 2013. 2006.
- [3] J. Zhang, W. Liu, and Z. Zhang, "Study on Characteristics Location of Pantograph-Catenary Contact Force Signal Based on Wavelet Transform," *IEEE Trans. Instrum. Meas.*, vol. 68, no. 2, pp. 402–411, 2019.
- [4] S. H. Kia, F. Bartolini, A. Mpanda-Mabwe, and R. Ceschi, "Pantograph-catenary interaction model comparison," *IECON Proc. Industrial Electron. Conf.*, pp. 1584–1589, 2010.
- [5] A. Collina and S. Bruni, "Numerical simulation of pantograph-overhead equipment interaction," *Veh. Syst. Dyn.*, vol. 38, no. 4, pp. 261–291, 2002.
- [6] O. Lopez-Garcia, A. Carnicero, and V. Torres, "Computation of the initial equilibrium of railway overheads based on the catenary equation," *Eng. Struct.*, vol. 28, no. 10, pp. 1387–1394, 2006.
- [7] M. Tur, E. García, L. Baeza, and F. J. Fuenmayor, "A 3D absolute nodal coordinate finite element model to compute the initial configuration of a railway catenary," *Eng. Struct.*, vol. 71, pp. 234–243, 2014.
- [8] Y. Song, Z. Liu, H. Wang, X. Lu, and J. Zhang, "Nonlinear modelling of high-speed catenary based on analytical expressions of cable and truss elements," *Veh. Syst. Dyn.*, vol. 53, no. 10, pp. 1455–1479, 2015.
- [9] Y. Song, Z. Liu, F. Duan, X. Lu, and H. Wang, "Study on wind-induced vibration behavior of railway catenary in spatial stochastic

- wind field based on nonlinear finite element procedure," *J. Vib. Acoust. Trans. ASME*, vol. 140, no. 1, pp. 011010-1-14, 2018.
- [10] Y. Song, Z. Liu, H. Wang, J. Zhang, X. Lu, and F. Duan, "Analysis of the galloping behaviour of an electrified railway overhead contact line using the non-linear finite element method," *Proc. Inst. Mech. Eng. Part F J. Rail Rapid Transit*, vol. 232, no. 10, pp. 2339-2352, 2018.
- [11] Z. Wang, Y. Song, Z. Yin, R. Wang, and W. Zhang, "Random Response Analysis of Axle-Box Bearing of a High-Speed Train Excited by Crosswinds and Track Irregularities," *IEEE Trans. Veh. Technol.*, vol. 68, no. 11, pp. 10607-10617, 2019.
- [12] Y. Song, P. Antunes, J. Pombo, and Z. Liu, "A methodology to study high-speed pantograph-catenary interaction with realistic contact wire irregularities," *Mech. Mach. Theory*, vol. 4, pp. 103940.
- [13] Y. Song, Z. Liu, A. Rønquist, P. Navik, and Z. Liu, "Contact Wire Irregularity Stochastics and Effect on High-speed Railway Pantograph-Catenary Interactions," *IEEE Trans. Instrum. Meas.*, 2020, doi: 10.1109/tim.2020.2987457.
- [14] Y. Song, Z. Liu, and X. Lu, "Dynamic Performance of High-Speed Railway Overhead Contact Line Interacting With Pantograph Considering Local Dropper Defect," *IEEE Trans. Veh. Technol.*, vol. 69, no. 6, pp. 5958-5967, 2020.
- [15] H. Wang, A. Núñez, Z. Liu, Y. Song, F. Duan, and R. Dollevoet, "Analysis of the evolution of contact wire wear irregularity in railway catenary based on historical data," *Veh. Syst. Dyn.*, vol. 56, no. 8, pp. 1207-1232, 2018.
- [16] P. Návík, A. Rønquist, and S. Stichel, "Identification of system damping in railway catenary wire systems from full-scale measurements," *Eng. Struct.*, vol. 113, pp. 71-78, 2016.
- [17] Y. Park, K. Lee, S. Y. Park, J. Y. Park, and W. S. Choi, "Implementation of multi-functional type condition monitoring system for railway catenary systems," *Trans. Korean Inst. Electr. Eng.*, vol. 64, no. 9, pp. 1406-1410, 2015.
- [18] Y. Song, Z. Liu, F. Duan, Z. Xu, and X. Lu, "Wave propagation analysis in high-speed railway catenary system subjected to a moving pantograph," *Appl. Math. Model.*, vol. 59, pp. 20-38, 2018.
- [19] A. Facchinetti and M. Mauri, "Hardware-in-the-loop overhead line emulator for active pantograph testing," *IEEE Trans. Ind. Electron.*, vol. 56, no. 10, pp. 4071-4078, 2009.
- [20] J. R. Jimenez-Octavio, A. Carnicero, C. Sanchez-Rebollo, and M. Such, "A moving mesh method to deal with cable structures subjected to moving loads and its application to the catenary-pantograph dynamic interaction," *J. Sound Vib.*, vol. 349, pp. 216-229, 2015.
- [21] Y. Song, Z. Liu, Z. Xu, and J. Zhang, "Developed moving mesh method for high-speed railway pantograph-catenary interaction based on nonlinear finite element procedure," *Int. J. Rail Transp.*, vol. 7, no. 3, pp. 173-190, 2019.
- [22] S. Gregori, M. Tur, A. Pedrosa, J. E. Tarancón, and F. J. Fuenmayor, "A modal coordinate catenary model for the real-time simulation of the pantograph-catenary dynamic interaction," *Finite Elem. Anal. Des.*, vol. 162, no. January, pp. 1-12, 2019.
- [23] P. Návík, A. Rønquist, and S. Stichel, "The use of dynamic response to evaluate and improve the optimization of existing soft railway catenary systems for higher speeds," *Proc. Inst. Mech. Eng. Part F J. Rail Rapid Transit*, vol. 230, no. 4, pp. 1388-1396, 2015.
- [24] Z. Xu, Y. Song, and Z. Liu, "Effective Measures to Improve Current Collection Quality for Double Pantographs and Catenary Based on Wave Propagation Analysis," *IEEE Trans. Veh. Technol.*, vol. 69, no. 6, pp. 6299-6309, 2020.
- [25] K. Lee and J. Chung, "Dynamic analysis of a hanger-supported beam with a moving oscillator," *J. Sound Vib.*, vol. 332, no. 13, pp. 3177-3189, 2013.
- [26] S. Bruni *et al.*, "The results of the pantograph-catenary interaction benchmark," *Veh. Syst. Dyn.*, vol. 53, no. 3, pp. 412-435, 2015.
- [27] P. Návík, A. Rønquist, and S. Stichel, "Variation in predicting pantograph-catenary interaction contact forces, numerical simulations and field measurements," *Veh. Syst. Dyn.*, vol. 55, no. 9, pp. 1265-1282, 2017.
- [28] A. Collina, S. Melzi, and A. Facchinetti, "On the prediction of wear of contact wire in OHE lines: A proposed model," *Veh. Syst. Dyn.*, vol. 37, no. SUPPL., pp. 579-592, 2003.
- [29] D. Zou, N. Zhou, L. Rui Ping, G. M. Mei, and W. H. Zhang, "Experimental and simulation study of wave motion upon railway overhead wire systems," *Proc. Inst. Mech. Eng. Part F J. Rail Rapid Transit*, vol. 231, no. 8, pp. 934-944, 2017.

- [30] Z. Liu, H. Wang, R. Dollevoet, Y. Song, A. Nunez, and J. Zhang, "Ensemble EMD-Based Automatic Extraction of the Catenary Structure Wavelength from the Pantograph-Catenary Contact Force," *IEEE Trans. Instrum. Meas.*, vol. 65, no. 10, pp. 2272-2283, 2016.



Yang Song (S'16-M'19) received a Ph.D. degree from Southwest Jiaotong University, Sichuan China, in 2018. He worked as a Research Fellow with the Institute of Railway Research, University of Huddersfield, UK from 10/2018 to 09/2019. He is currently a postdoctoral researcher in the Department of Structural Engineering, Norwegian University of Science and Technology, Norway. His research interests involve the assessment of railway pantograph-catenary interactions, the wind-induced vibration of long-span structures in railway transportation and coupling dynamics in railway engineering.



Anders Rønquist received a Ph.D. degree from Norwegian University of Science and Technology, Trondheim, Norway, in 2005. He is currently a full professor in the Department of Structural Engineering, Norwegian University of Science and Technology. His research interests include structural dynamics, wind engineering, structural monitoring and system identification for electric railways.



Petter Návík received a Ph.D. degree from Norwegian University of Science and Technology, Trondheim, Norway, in 2016. He is currently employed as a Postdoctoral Researcher in the structural dynamics group at the Department of Structural Engineering, Norwegian University of Science and Technology, NTNU. His research interests include structural dynamics, the dynamics of railway catenary systems, structural monitoring, operational modal analysis, and finite element modelling.